Astron. Astrophys. 357, 233–240 (2000)

ASTRONOMY AND ASTROPHYSICS

Wolf-Rayet wind structure and optical variability

Q. Li[1,5], **J.C. Brown**[1,2,3,4], **R. Ignace**[1,⋆], **J.P. Cassinelli**[1,4], **and L.M. Oskinova**[1,6]

[1] Department of Physics and Astronomy, University of Glasgow, Glasgow, G12 8QQ, Scotland, UK
[2] Astronomical Institute A. Pannekoek, University of Amsterdam, The Netherlands
[3] Institute of Astronomy, ETH Zürich, Switzerland
[4] Department of Astronomy, University of Wisconsin-Madison, USA
[5] Department of Astronomy, Beijing Normal University, P.R. China
[6] Astronomical Institute, University of St. Petersburg, Russia

Received 3 December 1999 / Accepted 8 March 2000

Abstract. Results are presented on the expected variability of Wolf-Rayet (WR) stars in broad-band optical polarimetry and photometry, and in emission line profiles, due to an inhomogeneous random distribution of blobs in spherical geometry. Time dependent $3-D$ simulations are carried out with blob ejection random in time and direction, and the radiation properties are evaluated in the optically thin limit. In contrast with previous purely statistical analyses, inclusion in the present treatment of a β velocity law and stellar occultation effects can yield results consistent with observations of the mean polarisation $\bar{p}$ and the ratio $\mathcal{R} = \sigma_{\rm p}/\sigma_{\rm phot}$ of polarimetric to photometric variability. Such consistency puts constraints on model parameters. Indeed by considering combinations of the three observables $\sigma_{\rm p}$, $\sigma_{\rm phot}$, and $\bar{p}$ it is possible to infer reasonably good estimates of three wind-blob parameters – the β of their velocity law, the total mass loss rate $\dot{M}$ in blobs and the total number $\mathcal{N}$ of blobs emitted per wind flow time (R_*/v_∞), provided the blobs are reasonably localised in angular and radial extent. It is found that typical data requires $\beta \geq 1.5$, $\mathcal{N} \approx 20$–50 and $\dot{M} \approx 10^{-4} M_\odot$/year. The $\mathcal{N}$ estimate is consistent with the number of observed narrow features on emission lines. Smaller values of β are excluded. This improved model shows that data do not after all demand very dense blobs as previously suggested, and offers a valuable diagnostic of WR wind structure parameters.

Key words: polarization – stars: mass-loss – stars: variables: general – stars: Wolf-Rayet – stars: winds, outflows

1. Introduction

Evidence for stochastic blob ejection from hot stars into their circumstellar winds has accumulated from a variety of spectropolarimetric studies, with variability appearing at a broad range of timescales. Lupie & Nordsieck (1987) presented low resolution polarisation data of long term (∼months) variations in a sample of OB supergiants. Taylor et al. (1991) found substantial and random polarimetric fluctuations occurring in P Cygni over a two year span. The data is sparse and irregularly spaced in time, but changes occur on scales of days, weeks, and months. More relevant for the results discussed in this paper, the Montreal group have amassed a large data set for polarimetric variability in Wolf–Rayet stars (e.g., St.-Louis et al. 1987; Drissen et al. 1987, 1992; Robert et al. 1989). Detailed data on the photometric, polarimetric, and spectral line profile variability of WR stars have been presented by Robert (1992) and Moffat & Robert (1992). Moffat & Robert (1992) and Lepine & Moffat (1999) have interpreted these phenomenologically in terms of a distribution of dense blobs in the wind which they suggest may result from hierarchical turbulence, while Brown et al. (1995) have discussed some of the physical properties of the larger blobs which dominate aspects of the data. Brown (1994) and Brown et al. (2000) have shown that blob formation by redistribution of electrons within the wind does not lead to polarimetric or photometric variability unless the redistribution occurs on large spatial scales or leads to very dense blobs. They conclude that blobs arise either by localised mass loss enhancements at the stellar surface or by the action of radiatively driven shocks sweeping up material on large scales. In the present paper we focus on the former case and concentrate on issues of blob velocity law and generation rate, though the ideas are generalisable to the latter situation.

A statistic of special interest found by Robert (1992) is that the broad band polarimetric variation $\sigma_{\rm p}$ is much smaller than the fractional photometric variability $\sigma_{\rm phot}$, the mean ratio being about $\mathcal{R} = \sigma_{\rm p}/\sigma_{\rm phot} \approx 0.05$. If the variability in both modes were solely due to electron scattering in a small number of blobs then, for simple geometries at least, one might expect a ratio $\mathcal{R}$ nearer unity. This discrepancy led Richardson et al. (1996) to investigate the statistical effect of having larger numbers of blobs present. They did so analytically and numerically by distributing blobs (of specified mean number N_o) randomly in distance and direction around the star. While they found $\mathcal{R}$ to decrease with N_o, it never became as small as 0.05 no matter how large N_o was. Richardson et al. (1996) concluded that the blobs must be

Send offprint requests to: john@astro.gla.ac.uk; li@astro.gla.ac.uk
⋆ Now at Department of Physics and Astronomy, University of Iowa, USA

very dense so that their emission ($\propto n^2 V$) is large enough to increase $\sigma_{\rm phot}$ and/or their optical depth is large enough to reduce $\sigma_{\rm p}$ by multiple scattering. In this paper we revisit and improve on this analysis by carrying out numerical simulations, following blob flow from the star with a β velocity law and allowing for the occultation of blobs behind the stellar disk. Note however that we retain the single scattering assumption. In Sect. 2, we define the basic geometry, parameters, and assumptions of the model and explain our algorithm for ejection of blobs randomly in angle and time. In Sect. 3 we present the results of our simulations and in Sect. 4 we relate them to observations and derive wind blob parameters from typical data. In particular we show that the conclusion of Richardson et al. (1996), that high blob density is essential to match variability data, arose from their implicit assumption of constant blob velocity. For large enough velocity index $\beta \approx 1.5$–2 our model allows matching of the data without dense blob multiple scattering or continuum emission being invoked. Valuable constraints on blob velocity law, ejection rate and mass loss rate can be inferred from the observed mean polarisation $\bar{p}$ and the polarimetric and photometric variances, especially when linked to the number of distinct narrow features in emission line profiles.

2. Model of polarisation and scattering from blobs

We assume that the polarimetric and photometric variability of WR stars is due to localised mass loss density enhancements which are generated at random positions at the stellar surface and at random time intervals with a normal distribution of mean value Δt. The blobs are then taken to move radially outward with a velocity law, and constant solid angle $\Delta\Omega$ and radial thickness Δr, the uniform electron density then decreasing as $r^{-2}\, v^{-1}(r)$. (This assumption of constant $\Delta\Omega$ and Δr has little effect on the results). The blobs thus have axisymmetric shapes and, on the assumption that they are not optically thick in the continuum, the results of Brown & McLean (1977) can be used to find the polarisation of a single blob as:

$$p = \tau_{\rm opt}\,(1\text{–}3\gamma)\sin^2 i, \tag{1}$$

where

$$\tau_{\rm opt} = \frac{3}{16}\sigma_{\rm T}\int_{r_1}^{r_2}\int_{\mu_2}^{\mu_1} n(r,\mu)\,dr\,d\mu \tag{2}$$

is a mean optical depth, and

$$\gamma = \frac{\int_{r_1}^{r_2}\int_{\mu_2}^{\mu_1} n(r,\mu)\mu^2\,dr\,d\mu}{\int_{r_1}^{r_2}\int_{\mu_2}^{\mu_1} n(r,\mu)\,dr\,d\mu} \tag{3}$$

is a "shape" factor. i is the blob axis inclination to the line of sight; $\mu = \cos\vartheta$, where ϑ is the blob opening angle between the axis of symmetry and the direction of the scatterer seen from the center of the star; $n(r,\mu)$ is the electron number density in the blob; and $\sigma_{\rm T}$ is the Thomson scattering cross-section. For the local reference frame (r,ϑ) chosen, we let $\mu_1 = 1$. For constant solid angle $\Delta\Omega = 2\pi\,(1-\mu_2)$ and radial extent Δr, the electron density is assumed to vary only with radius inside the blob i.e. as $n(r,\mu) = n(r)$. In order to calculate the electron density in one blob, we can use the mass conservation law:

$$\dot{M}_b = \Delta\Omega\, r^2\, \rho(r)\, v(r) \tag{4}$$

where $\dot{M}_b$ is the mass outflow rate within one blob, $\rho(r)$ is the mass density, and $v(r)$ is the blob velocity law which we adopt to be of the common form:

$$v(r) = v_\infty\left(1 - \frac{b\,R_*}{r}\right)^\beta \tag{5}$$

where v_∞ is the terminal wind speed, R_* is the radius of the WR star, b is a dimensionless parameter to ensure that the initial wind speed is non-zero, and β is a velocity law index. In our simulations we adopt $b = 0.995$. We note that in using a β-law (5) for $v(r)$, it is in practice essential to use it in a form with a finite $v = v_o$ at the wind base since for larger β values blobs would otherwise take an infinite time to reach finite $r - R_*$. This can be done either by setting $v = v_o$ at $r = R_*$ (which is effectively what we do through the parameter b) or by starting material at $r = R_*(1+\epsilon)$, with $\epsilon \ll 1$. We experimented with the value of v_o/v_∞ and found that our results as a function of β were insensitive to v_o/v_∞ so long as it was small. This is a little surprising since small v_o/v_∞ causes a blob to dwell longer near the star, as does finite β. However, for very small v_o/v_∞ the effect of this is to delay the blob for many flow times very near $r = R_*$. This will increase the value of $f_{\rm s}$ (which is not measurable anyway) but not of $\bar{p}$ since the depolarisation factor is near zero. But, the travel time in this region is much longer than a flow time, so blobs there will affect the time variances very little. The effect of β on the dwell time, however, is felt further (around $r = 2R_*$) out where the speed and effect on variations is larger, and so dominates the effect of the $v(r)$ law parameters on the observables.

The blob electron density becomes

$$\begin{aligned} n_e &= \frac{\rho}{\mu_e\, m_H} \\ &= \frac{\dot{M}_b}{\mu_e\, m_H\, \Delta\Omega\, r^2\, v} \\ &= \frac{\dot{M}_b}{\mu_e\, m_H\, \Delta\Omega\, r^2\, v}. \end{aligned} \tag{6}$$

where m_H is the hydrogen mass and μ_e is the mean particle weight per free electron.

To incorporate the finite star geometry, the correction factors $D(r/R_*), C(r/R_*,\chi)$ can be employed according to Cassinelli et al. (1987) and Brown et al. (1989), viz.

$$\begin{aligned} D &= \sqrt{1 - \frac{R_*^2}{r^2}} \\ &= \sqrt{1 - \frac{1}{x^2}} \end{aligned} \tag{7}$$

and

$$C = \frac{8 - D(1+D)\,(1 - 3\cos^2\chi)}{3(1+D)(1+\cos^2\chi)} \tag{8}$$

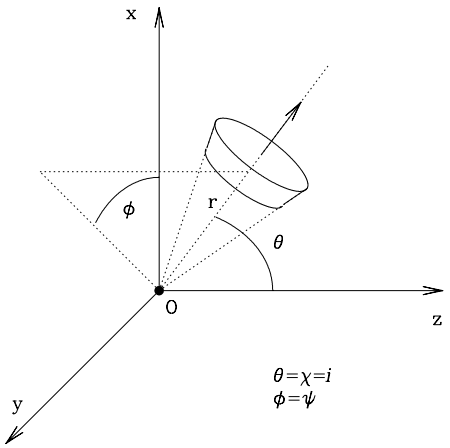

Fig. 1. Geometry of scattering from one blob. We employ a coordinate system (r, θ, ϕ) with oz along the line of sight. For each blob the "inclination" angle i is identical to the scattering angle χ and the polar angle θ, while the polarisation position angle ψ is just the coordinate component ϕ.

where $x = r/R_*$, again R_* is the photospheric radius of the WR star, and $\chi = i$ is the viewing inclination.

We now wish to combine Eqs. (1) to (8) to yield an expression for the polarisation from a single blob with the assumed geometry. Since the density does not vary with μ within the blob, the angle integrals in Eqs. (2) and (3) for $\tau_{\rm opt}$ and γ are straightforward. We also choose to rewrite the velocity in (5) as $v = v_\infty\,[x/(x-b)]^\beta]$. Combining, the polarisation expression now becomes

$$p = \frac{3}{16}\,\sigma_{\rm T}\,n_o\,R_*\,(1-\mu_2)(\mu_2+\mu_2^2)\sin^2\chi \times \int_{x_1}^{x_2}\left(\frac{x}{x-b}\right)^\beta \frac{D(x)\,dx}{x^2}, \quad (9)$$

and the scattered light intensity as a fraction $f_{\rm s}$ of $L_*/4\pi$ in terms of Brown et al. (1995) is:

$$f_{\rm s} = \frac{3}{16}\,\sigma_{\rm T}\,n_o\,R_*\,(1-\mu_2)\,(1+\cos^2\chi) \times \int_{x_1}^{x_2}\left(\frac{x}{x-b}\right)^\beta \frac{C(x,\chi)\,dx}{x^2}, \quad (10)$$

where $n_o = \dot{M}_b/(\mu_e\,m_H\,\Delta\Omega\,{R_*}^2\,v_\infty)$.

These expressions are for a single blob. To deal with the presence of many blobs, we use the coordinate system (r, θ, ϕ) with oz along the line of sight. Then for each blob the "inclination" angle i is identical to the scattering angle χ and the polar angle θ, while the polarization position angle ψ is just the coordinate component ϕ (see Fig. 1). For a system of blobs labelled $j = 1,\ N$, the total scattered light fraction $f_{\rm s}$ and the net polarisation are as usual simply given by summing over j the Stokes intensity parameters $Q_j = p_j \cos 2\phi_j$, $U_j = p_j \sin 2\phi_j$ of each to get the totals Q, U, then finding $p = (Q^2+U^2)^{1/2}$ and position angle $\Psi = \frac{1}{2}\arctan\frac{U}{Q}$. Blobs enter the flow in random directions such that $\mu_j = \cos\theta_j$ is uniformly sampled in the interval -1 to $+1$ and ϕ_j from 0 to 2π. The radii x_j are determined by time and the velocity law. The results are as follows, where it is to be understood that *summations exclude all occulted blobs* – i.e. blobs whose coordinates x_j, θ_j, ϕ_j satisfy $\theta_j > \pi/2$ and $x_j\,\sin\theta_j < 1$.

The time averaged total mass loss rate in all blobs in the inhomogeneous but mean spherical "wind" is $\dot{M} = \dot{N} N_e \mu_e m_H$, where $\dot{N}$ is the mean blob ejection rate ($\rm s^{-1}$) and N_e is the number of electrons in one blob. Thus, if we fix $\dot{M}$ and increase $\dot{N}$ then there are more blobs in any given range of r but each of smaller N_e with the structure approaching spherical symmetry as $\dot{N} \to \infty$. Usually, we denote $\mathcal{N} = \dot{N}\,\tau$, the number of blobs ejected per flow time ($\tau = R_*/v_\infty$), as the measure of the blob ejection rate.

The system of equations governing the time varying polarisation and scattered light is then

$$\begin{aligned} Q &= \sum_{j=1}^{N} Q_j \\ &= \frac{3}{16}\,\sigma_{\rm T}\,n_o\,R_*(1-\mu_2)(\mu_2+\mu_2^2)\sum_{j=1}^{N}\sin^2\theta_j\,\cos 2\phi_j \\ &\quad\times\int_{x_1}^{x_2}\left(\frac{x_j}{x_j-b}\right)^\beta \frac{1}{x_j^2}\sqrt{1-\frac{1}{x_j^2}}\,dx \end{aligned} \quad (11)$$

and

$$\begin{aligned} U &= \sum_{j=1}^{N} U_j \\ &= \frac{3}{16}\sigma_{\rm T}\,n_o\,R_*(1-\mu_2)(\mu_2+\mu_2^2)\sum_{j=1}^{N}\sin^2\theta_j\sin 2\phi_j \\ &\quad\times\int_{x_1}^{x_2}\left(\frac{x_j}{x_j-b}\right)^\beta \frac{1}{x_j^2}\sqrt{1-\frac{1}{x_j^2}}\,dx \end{aligned} \quad (12)$$

Hence

$$p = \sqrt{Q^2+U^2} \quad (13)$$

and

$$\begin{aligned} f_{\rm s} &= \sum_{j=1}^{N} f_{\rm sj} \\ &= \frac{3}{16}\sigma_{\rm T} n_o R_*(1-\mu_2)\sum_{j=1}^{N}(1+\cos^2\theta_j) \\ &\quad\times\int_{x_1}^{x_2}\frac{8-D_j(1+D_j)(1\text{–}3\cos^2\phi_j)}{3(1+D_j)} \\ &\quad\times\left(\frac{x_j}{x_j-b}\right)^\beta dx \end{aligned} \quad (14)$$

On inspection of the above equations for polarisation and scattered light, we expect that, for given $\dot{M}$, $\Delta\Omega$, Δr, and β, results should depend mainly on the mean time intervals $\Delta t = 1/\dot{N}$ between consecutive blobs as a fraction of the flow time τ - i.e. on $\mathcal{N}$. For fixed mass loss rate and flow time, if the blob

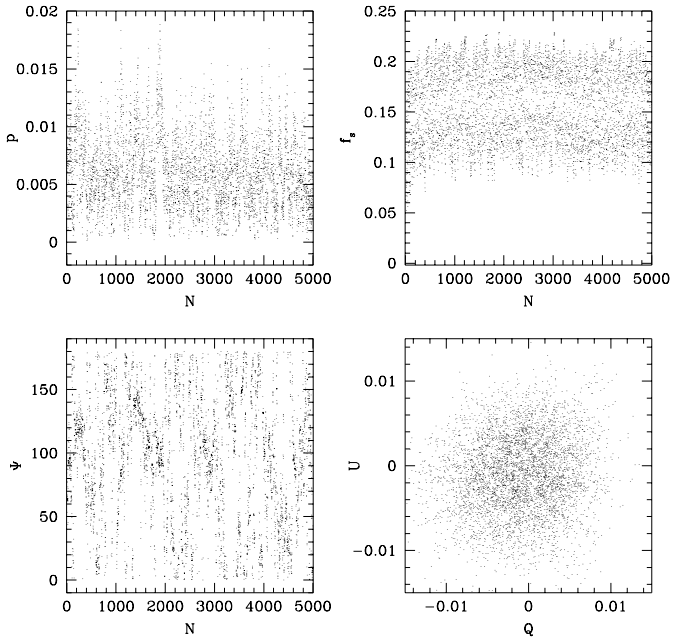

Fig. 2. The figures show respectively, instant by instant, model results versus number N of blobs emitted thus far for the following: upper left panel – polarisation p; upper right – scattered light $f_{\rm s}$; lower left panel – polarisation position angle ψ; lower right panel – Q(N) versus U(N). Parameters used throughout are: $\dot{M} = 10^{-4} M_{\odot}$/year, $R_* = 10 R_{\odot}$, $v_{\infty} = 1800\,{\rm km\,s^{-1}}$, $\Delta\Omega = 0.04$, $\mathcal{N} = 100$, and $\beta = 1$.

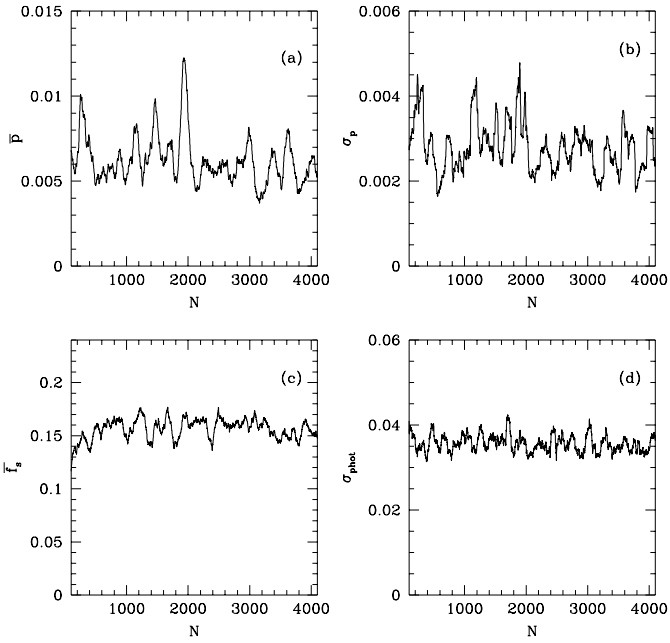

Fig. 3a–d. Based on the same data as Fig. 2, here we show smoothed results versus number of blobs N (increasing with time) for the following observables, with parameters as in Fig. 2: **a** mean polarisation $\bar{p}$; **b** variance of polarisation $\sigma_{\rm p}$; **c** mean scattered light fraction $\bar{f}_{\rm s}$; **d** variance of scattered light $\sigma_{\rm phot}$.

generation rate is low, only a few blobs each of large density will be present near the star and these will dominate the p and $f_{\rm s}$ values. However for high generation rates, many low density blobs near the star will be controlling p and $f_{\rm s}$. So the same total number of electrons is redistributed in different number of blobs, resulting in different statistical means and variances in the polarisation and scattered light fraction. For a fixed blob ejection and mass loss rate, the number of blobs in the inner radii near the star has a steady mean value and so therefore do the resulting polarisation, scattered intensity and their variances, but these values change with $\mathcal{N}$, $\dot{M}$, and β. So their observed values allow inference of the blob emission and flow parameters, as we now discuss.

3. Model results

1. By design, the model is in qualitative agreement with data showing photometric and polarimetric fluctuations about some mean values (see Robert 1992). Fig. 2 shows how typical polarisation, position angle, and scattered light fraction change with the total number of blobs emitted from the start – i.e with time, starting from ejection of the first blob, for the model with the indicated parameters. The observables all rise to steady mean values within the first few flow times, because thereafter the number of blobs near the star, which dominate the scattered light, becomes steady on average. Polarisation changes are also shown as a locus in the Q – U plane (see Fig. 2) which, as expected, shows no preferred direction, since the mean structure is spherical. In Fig. 3 we show "observational" time–smoothed results for the variations in mean polarisation and scattered light. We applied "boxcar" smoothing with a width of about one flow time (i.e., about 1 hour for the chosen star parameters). Standard deviations, σ, of these quantities are also plotted in Fig. 3.

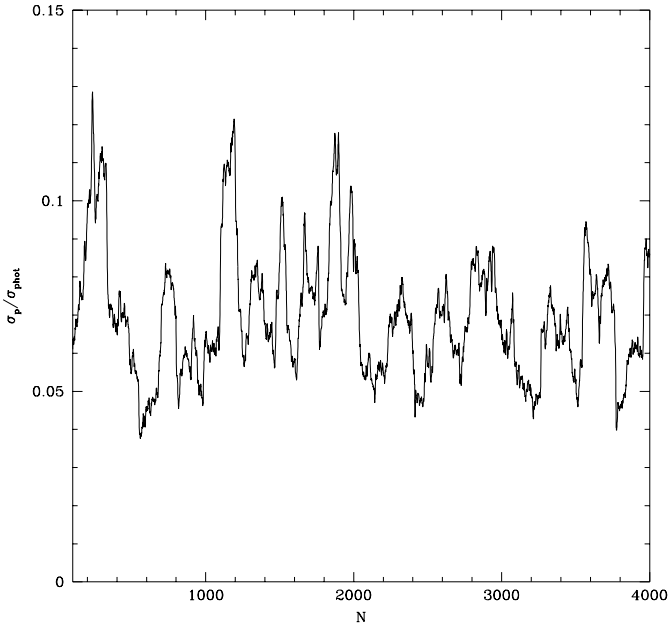

Fig. 4. Ratio ($\mathcal{R} = \sigma_{\rm p}/\sigma_{\rm phot}$) of polarimetric versus photometric standard deviations versus number of blobs N which are for the same parameters as in Fig. 2. The steady mean value of $\mathcal{R}$ is about 0.07 for these parameters.

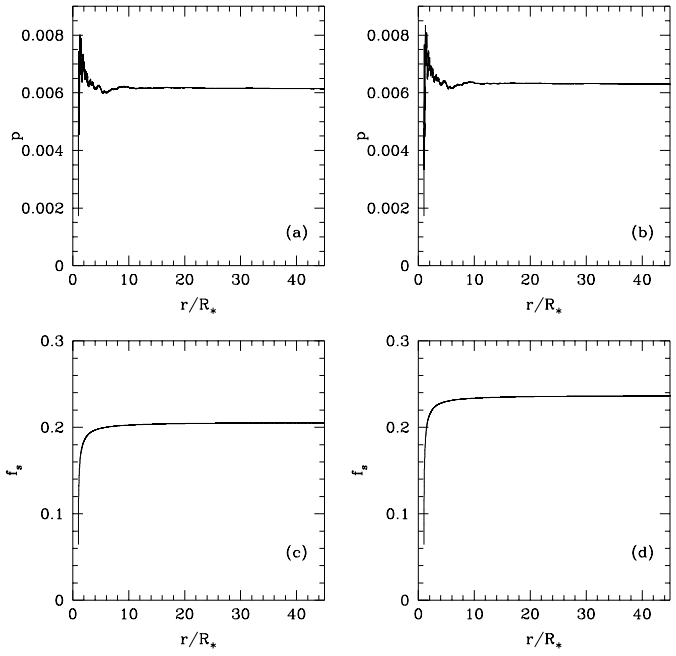

Fig. 5. Panels **a** and **b** show the values, with and without occultation, of the cumulative polarisation $p(r/R_*)$ at a certain moment due to all the blobs out to distance r from the star's center. Panels **c** and **d** similarly for the cumulative scattered light $f_{\rm s}(r/R_*)$. Model parameters are the same as Fig. 2. From these plots, it is clear that the blobs within a few R_* of the star dominate the observables. Fluctuations in p are mainly due to angular cancellation effects. Comparing occulted and unocculted cases, the latter have higher values of $f_{\rm s}$ as expected since more scatterers are visible, while p is somewhat increased since blobs nearly directly opposite the star have non-negligible polarisation.

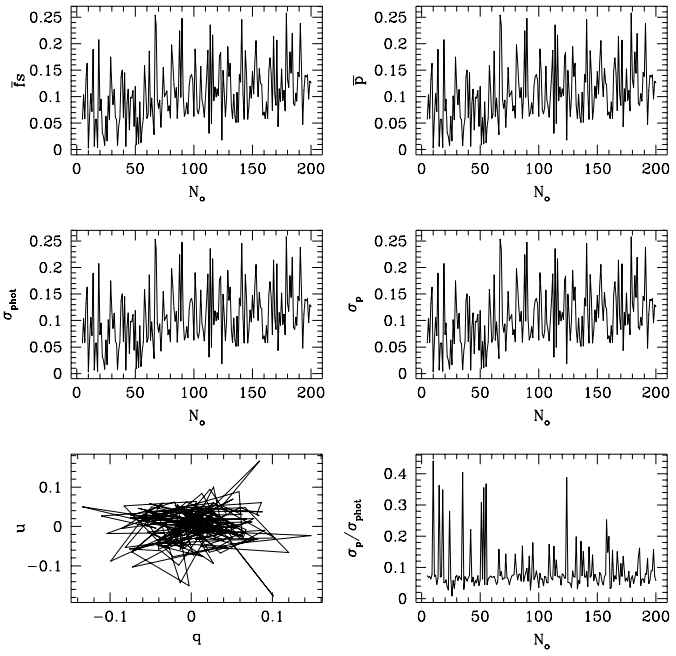

Fig. 6. These figures were created similarly to the work of Richardson et al. (1996), considering blobs to have random distances but weighted for a $\beta = 1$ velocity law, the total number of blobs at any instant being random with Poisson mean value N_o. Parameters have the same values as in previous figures. They show that our dynamic model gives similar results to the purely statistical approach.

Fig. 4 is the ratio $\mathcal{R}$ versus total number of blobs N as time progresses.

2. To confirm the dominance of inner blobs explicitly, we show the cumulative contributions of blobs to the polarisation and scattered light after a long time ($\gg 1/\dot{N}$) in Fig. 5. We find that only the blobs which are close to the star give significant contributions. That is, once enough blobs have entered the flow so that the inner few stellar radii contain a mean steady state number of blobs, then steady mean values for p, $f_{\rm s}$, $\sigma_{\rm p}$, and $\sigma_{\rm phot}$ are achieved, because the distant blobs are irrelevant and give only small contributions (see Fig. 5). The effect of an accelerating velocity law $v(r)$ is that a larger effective number of blobs lies near the star for a given $\mathcal{N}$. Broadly speaking we expect that increasing $\dot{M}$ alone will increase mean values of p, $f_{\rm s}$ but will not change their relative σ, whereas varying $\mathcal{N}$ alone affects the variances. In the next section we discuss how these properties can be used to constrain β, $\dot{M}$, and $\dot{N}$ from data.
3. In the Richardson et al. (1996) analysis, θ_j, r_j, and N_{ej} were taken as randomly distributed so that in effect it was assumed that $v(r)$ was constant. The total number of blobs N was taken to be a random variable given by a Poisson distribution with a mean value N_o. They found that no mean number of blobs, N_o, could make $\mathcal{R} = \sigma_{\rm p}/\sigma_{\rm phot}$ as small (0.05) as observed. But when we consider a β velocity law for the blob motion, and allow for occultation of blobs behind the star (whose back – scattered light has small values of polarisation but large values of $f_{\rm s}$), we find using the same approach as they did, that results can match observed $\mathcal{R}$ for large enough β (see Fig. 6). (Note here we use the same definition for $\sigma_{\rm p} = (\sigma_Q^2 + \sigma_U^2)^{1/2}$ as Moffat & Robert 1992). We conclude that Richardson et al's constant velocity assumption limited their ability to reproduce the observed $\mathcal{R}$. In our modelling we treat the problem dynamically, following blob motion after ejection rather than the blob "snapshot" approach of Richardson et al. (1996), but the results from these two methods are consistent – our results essentially match theirs for $\beta = 0$ apart from minor differences due to their having a variation in blob numbers and sizes.
4. Results for "observables" as a function of $\mathcal{N}$ from our time–dependent $3-D$ model are shown in Table 1 with occultation effects included, for the values of $\dot{M}$, $\Delta\Omega$, Δr, β, etc., indicated. In each case we ran our code for 5000 blobs in total and for the same value of $\Delta\Omega = 0.04$ (equivalent to a cone semi-angle of roughly 7°). In Fig. 7 we show that results are relatively insensitve to $\Delta\Omega$ (unless we go to extreme values like 0 or 4π which yield zero polarisation by spherical symmetry). The same is also true of Δr which is the blob width. Fig. 8 shows the effects of varying $\dot{M}$. As expected, all absolute values of scattered light parameters p, $f_{\rm s}$ just scale linearly with $\dot{M}$ while the ratios of p, $f_{\rm s}$ and of their variances $\sigma_{\rm p}$, $\sigma_{\rm phot}$ are independent of $\dot{M}$. The effect

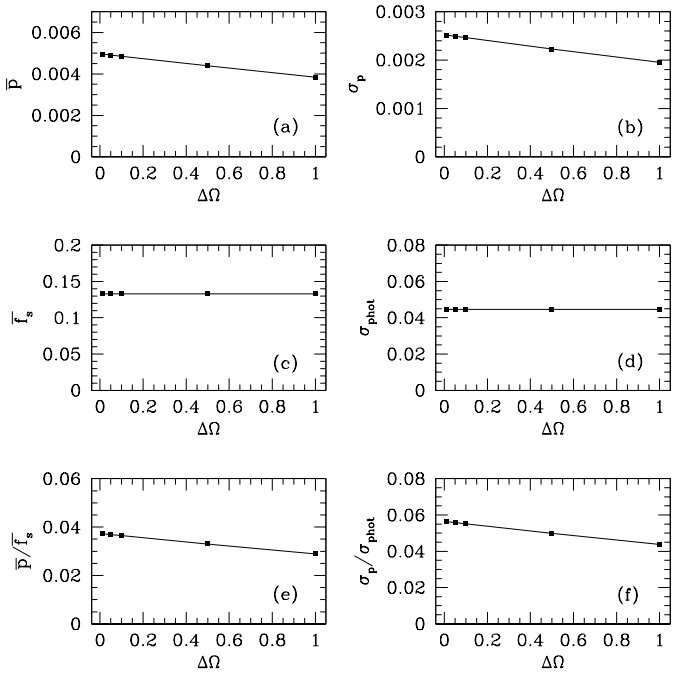

Fig. 7a–f. Effect on observables of varying the blob solid angle $\Delta\Omega$ for parameter values $\dot{M} = 10^{-4} M_\odot$/year, $R_* = 10R_\odot$, $v_\infty = 1800\,\mathrm{km\,s^{-1}}$, $\mathcal{N} = 100$, and $\beta = 1$. The points are for explicit model calculations.

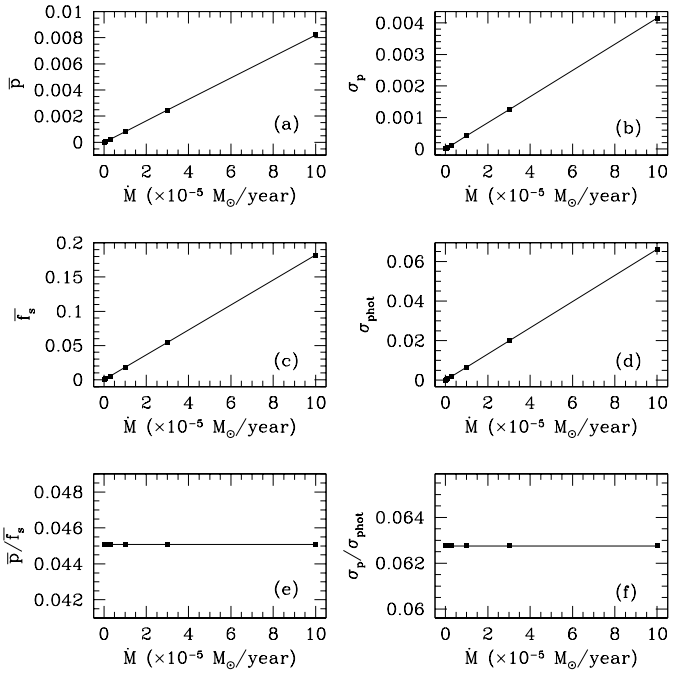

Fig. 8a–f. Effect on observables of varying $\dot{M}$. Panel **a** shows that $p \approx 0.5\%$ corresponds to $\dot{M} \approx 6 \times 10^{-5} M_\odot$/year for $\mathcal{N} = 100$. Panels **e** and **f** show that $\bar{p}/\bar{f}_\mathrm{s}$ and $\mathcal{R} = \sigma_\mathrm{p}/\sigma_\mathrm{phot}$ are independent of $\dot{M}$. Parameters used throughout are as follows: $\Delta\Omega = 0.04$, $R_* = 10R_\odot$, $v_\infty = 1800\,\mathrm{km\,s^{-1}}$, $\mathcal{N} = 100$, and $\beta = 1$.

Table 1. Simulation results for finite star source with occultation and velocity law

N	$\mathcal{N}$	$\bar{p}$	σ_p	$\bar{f}_\mathrm{s}$	σ_phot	$\bar{p}/\bar{f}_\mathrm{s}$	$\sigma_\mathrm{p}/\sigma_\mathrm{phot}$
5000	1/3	2.868	1.326	3.226	1.219	0.953	0.769
5000	1	1.475	0.429	2.882	0.722	0.511	0.594
5000	2	0.088	0.080	1.801	1.612	0.049	0.049
5000	5	0.039	0.030	0.735	0.645	0.053	0.047
5000	10	0.021	0.014	0.407	0.323	0.052	0.043
5000	20	0.014	0.007	0.255	0.160	0.053	0.045
5000	50	0.008	0.004	0.182	0.066	0.045	0.063
5000	100	0.0056	0.0028	0.1601	0.0362	0.035	0.076
5000	150	0.0047	0.0023	0.1491	0.0262	0.032	0.087
5000	200	0.0039	0.0019	0.1480	0.0211	0.026	0.090
5000	250	0.0036	0.0018	0.1444	0.0182	0.025	0.096
5000	300	0.0032	0.0014	0.1431	0.0145	0.022	0.096
5000	400	0.0027	0.0013	0.1421	0.0133	0.019	0.098

Notes: The following parameters are employed in the simulations: $\dot{M} = 10^{-4} M_\odot$/year, $\Delta\Omega = 0.04$, $\Delta r = 0.01 R_*$, $R_* = 10R_\odot$, $v_\infty = 1800\,\mathrm{km\,s^{-1}}$, and $\beta = 1$.

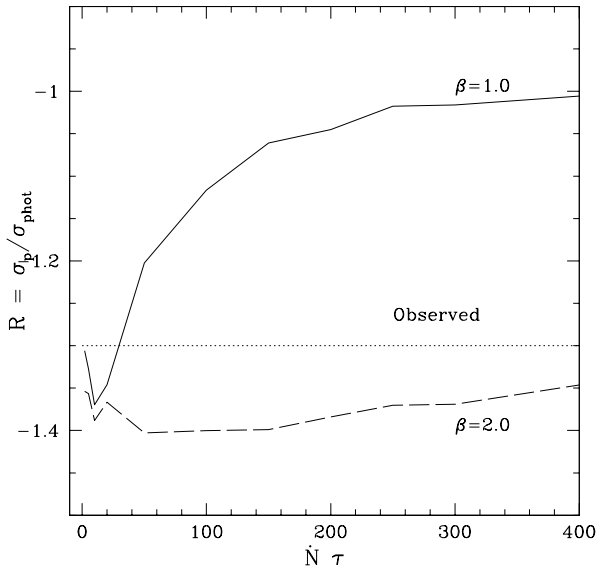

Fig. 9. Figure shows $\mathcal{R} = \sigma_\mathrm{p}/\sigma_\mathrm{phot}$ versus $\mathcal{N}$. Here $\mathcal{N} = \dot{N}\,\tau$ and τ is the flow time. The horizontal dotted line is the observed ratio. Parameters used throughout are as follows: $\dot{M} = 10^{-4} M_\odot$/year, $\Delta\Omega = 0.04$, $R_* = 10R_\odot$, $v_\infty = 1800\,\mathrm{km\,s^{-1}}$.

of occultation is not very large except for small $\mathcal{N}$. The reason is that only a few blobs are near the star in the small $\mathcal{N}$ case, so that the occasional occultation of a blob can have a dramatic effect on the observables.

From Table 1, we can see that in the first three rows, the polarisation and scattered light exceed unity due to the high blob density and optical depth for small $\mathcal{N}$, so that our model violates its single scattering basis for very low blob ejection and high mass loss rates but is otherwise self-consistent.

5. Fig. 9 shows that for different β, we get different $\mathcal{R}$ versus $\mathcal{N}$ curves with $\mathcal{R}$ going to near constant values for large $\mathcal{N}$. The larger the β we have, the lower that $\mathcal{R}$ becomes. The reason is that large β implies more blobs near the star where p, σ_p are small due to finite light source size. That is

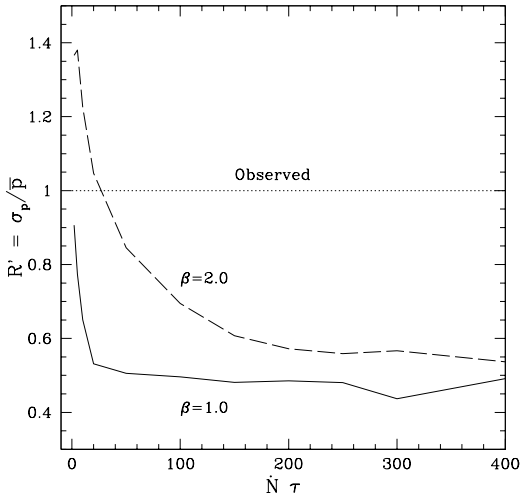

Fig. 10. A plot of $\mathcal{R}' = \sigma_{\rm p}/\bar{p}$ curves versus $\mathcal{N}$ for different velocity laws β but with the same parameters used in Fig. 9. The horizontal dotted line is the observed ratio. Velocity laws with $\beta < 1$ appear to be excluded. Comparison of the observed ratios $\mathcal{R}$ and $\mathcal{R}'$ of Fig. 9 and this figure appear consistent with $1.5 < \beta < 2$ and $\mathcal{N}$ in the range 20–50.

why Richardson et al. (1996) could not get $\mathcal{R}$ as small as observed using a constant velocity.

4. Application to data

From the results of Sect. 3 it is clear that for a fixed number $\mathcal{N}$ of blobs per flow time, the mean level and variances of scattered light and polarisation scale up as the total mass loss rate $\dot{M}$ is increased, simply because there are more scatterers. On the other hand, the relative degree of variability and of polarimetric cancellation are mainly governed by the number of blobs lying within a few stellar radii – which is fixed by $\mathcal{N}$, the ejection rate of blobs per flow time, and by the velocity law β value. More distant blobs do not contribute much to the scattering (see Fig. 5). Due to increased angular cancellation, to achieve a prescribed mean polarisation, as $\mathcal{N}$ is increased a larger total number of blob electrons (and hence total mass) has to be emitted per second by the star. The effect of occultation is mainly to hide backward scattering electrons which contribute little to p but significantly to $f_{\rm s}$ so reducing $\mathcal{R}$. When combined with the full 3–D treatment of blob distribution geometry, this in fact can bring results into compatibility with data for suitably chosen model parameters and can indeed be used as a means to infer wind parameters, as we now show.

The observable photometric and polarimetric variability quantities related to clumpy winds are essentially $\sigma_{\rm p}$ and $\sigma_{\rm phot}$ plus $\bar{p}$ if the interstellar and ambient polarisations are either zero or known. (Mean scattered light $f_{\rm s}$ is not really an observable since it is difficult to distinguish from direct starlight). Because $\dot{M}$ primarily determines the absolute value of $\bar{p}$ while $\mathcal{N}$ mainly governs $\mathcal{R} = \sigma_{\rm p}/\sigma_{\rm phot}$, we can use data on $\bar{p}$ and $\mathcal{R}$ to set limits on $\dot{M}$ and $\mathcal{N}$ using Figs. 7 to 10.

We thus ideally have a set of three observables $(\sigma_{\rm p}, \sigma_{\rm phot}, \bar{p})$ and the blobby wind model is largely controlled by three parameters $[\dot{M}, \dot{N}({\rm or}\,\mathcal{N}), \beta]$ since we have found results to be insensitive to $\Delta\Omega$ and Δr over likely value ranges. It is thus of interest to see whether we can determine these parameters from the observables. We first note that since $(\sigma_{\rm p}, \sigma_{\rm phot}, \bar{p})$ all scale linearly with $\dot{M}$ for fixed $(\mathcal{N})$ and (β), we can initially set $\dot{M}$ aside if we consider only the ratios $\mathcal{R} = \sigma_{\rm p}/\sigma_{\rm phot}$ as previously defined and also the ratio $\mathcal{R}' = \sigma_{\rm p}/\bar{p}$ shown in Figs. 9 and 10 for various β.

Typical observed values from Robert (1992) are $\bar{p} \approx 0.5\%$, $\sigma_{\rm p} \approx 0.5\%, \sigma_{\rm phot} \approx 10\%$ so that $\mathcal{R} \approx 0.05$ and $\mathcal{R}' \approx 1.0$. We see from Fig. 9 that for small values of $\beta \ll 1$ it is only possible to match the observed value or $\mathcal{R}$ for very small $\mathcal{N}$ but these are excluded by the number of narrow features seen in WR emission lines, as discussed further below. For $\beta \geq 1$ or so, the $\mathcal{R}$ value can be matched for a wide range of $\mathcal{N}$ including larger values (greater than about 20) consistent with the emission features. Excluding low $\beta(\leq 1)$ on this basis we turn to $\mathcal{R}'$ in Fig. 10, where we see that $\mathcal{R}'$ $\approx$1 excludes all β below about 1.5 and that for $\beta \approx 1.5$–2.0 we have to have $\mathcal{N} \approx$ 20–40. These bounds on β provide an important confirmation of independent estimates from spectrometry. We note that the constraint from $\mathcal{R}'$ is weaker than that from $\mathcal{R}$ in that the model values of $\mathcal{R}' = \sigma_{\rm p}/\bar{p}$ assumes that the observed $\bar{p}$ is solely due to the blobs, and that any constant interstellar or intrinsic polarisation (e.g. due to a flattened smooth wind) has been removed. A smaller value of $\bar{p}$ associated with the blobs alone would push our solution toward larger β and/or smaller $\mathcal{N}$ though the latter is quite tightly limited by the number of narrow emission line features discussed below. If we now return to the absolute value of $\bar{p}$ and again assume it is solely due to the blobs, we can estimate the $\dot{M}$ needed to achieve this $\bar{p}$ for the value or range of values estimated for β, $\mathcal{N}$ from $\mathcal{R}$, $\mathcal{R}'$ as discussed above.

However, for a given $\beta \geq 1$, we also see that any value of $\mathcal{N} \geq 20$ is consistent with the observed $\mathcal{R}$ but with increasing $\mathcal{N}$ the value of $\dot{M}$ needed to achieve $\bar{p} = 0.5\%$ becomes unreasonably large both on physical grounds and to be consistent with the single scattering limitation on p. Specifically for $\beta = 1$ and $\mathcal{N} = 20$, 100, and 400 we find respectively $\dot{M} = 4\times10^{-5} M_\odot$/year, $10^{-4} M_\odot$/year, and $2\times10^{-4} M_\odot$/year, so that the range $\mathcal{N} \approx$ 20–50 is again suggested as most plausible and in line with other estimates of WR star $\dot{M}$ values.

Another constraint on $\mathcal{N}$ comes from the emission line profile features produced by the blobs (see Robert 1992). A very high rate $\mathcal{N}$ will produce many narrow features which will blend to produce a smooth broad profile, like that from a smooth spherical wind (c.f., Brown et al. 1998) lacking the narrow features actually observed on top of a smooth profile. A very small $\mathcal{N}$ on the other hand would produce only a few narrow emission line features without the observed smooth underlying profile. To see whether the emission line profile for our estimated range of $\mathcal{N}$ resembles actual data, we have crudely modelled the line profile by taking each blob to emit at a total rate $\propto n^2 V \propto r^{-2}$ for constant radial thickness, centred

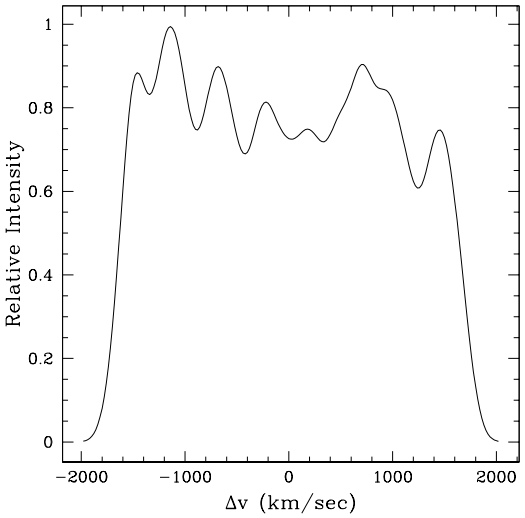

Fig. 11. Narrow feature contributions from all blobs to a wind emission line profile (wavelength shift in velocity units). Parameters are $\dot{M} = 10^{-4} M_\odot$/year, $R_* = 10 R_\odot$, $v_\infty = 1800\,\mathrm{km\,s^{-1}}$, $\mathcal{N} = 50$, and $\beta = 1$. Plot corresponds to a randomly chosen observational instant.

at a wavelength shift $\Delta\lambda/\lambda_o = v\cos\theta/c$ and broadened with Gaussian spread which we chose to be $\Delta\lambda/\lambda_o = 0.1v/c$ chosen rather arbitrarily to represent velocity turbulence and gradient effects – both much larger than thermal broadening. In Fig. 11, we show the profile at a random time for the case $\mathcal{N} = 50$. We see that about ten distinct narrow features are present at any random time, consistent with Robert's (1992) results. This is governed by the degree of blending resulting from our assumed narrow feature broadening, but shows that the line profiles observed are broadly consistent with $\mathcal{N} \approx 20$–50 for our assumed smearing.

In summary our approach provides a valuable new means of studying blob ejection, mass loss rates, and also the blob velocity law in WR winds and should enable further insight into blob production processes. Other work in progress will address the relationship of these results to other hot wind signatures such as X-ray variability.

Acknowledgements. Appreciation is expressed to the referee, G. Hill, for a careful reading and clarifying comments that have improved this paper. The authors acknowledge support for this work from: U.K. PPARC Research and Visiting Fellowship Grants (JCB, RI, JPC); China Scholarship Council (QL); ETH Zurich and University of Amsterdam Visitor Funds (JCB); a NASA grant (JCB, JPC, QL); and a Royal Society/NATO Exchange Fellowship (LMO).

References

Brown J.C., 1994, In: Moffat A.F.J., St-Louis N. (eds.) Quebec Workshop on Instability and Variability in Hot Star Winds. Ap&SS 221, 357
Brown J.C., McLean I.S., 1977, A&A 57, 141
Brown J.C., Carlaw V.A., Cassinelli J.P., 1989, AJ 344, 341
Brown J.C., Richardson L.L., Antokhin I., et al., 1995, A&A 295, 725
Brown J.C., Richardson L.L., Ignace R., Cassinelli J.P., 1998, A&A 330, 253
Brown J.C., Ignace R., Cassinelli J.P., 2000, A&A 356, 619
Cassinelli J.P., Nordsieck K.H., Murison M.A., 1987, ApJ 317, 290
Drissen L., St.-Louis N., Moffat A.F.J., Bastien P., 1987, ApJ 322, 888
Drissen L., Robert C., Moffat A.F.J., 1992, ApJ 386, 288
Lepine S., Moffat A.F.J., 1999, ApJ 514, 909
Lupie O.L., Nordsieck K.H., 1987, AJ 92, 214
Moffat A.F.J, Robert C., 1992, ASP No. 22, 203
Richardson L.L., Brown J.C., Simmons J.F.L., 1996, A&A 306, 519
Robert C., 1992, Ph.D. Thesis, Univ. de Montreal
Robert C., Moffat A.F.J., Bastien P., Drissen L., St.-Louis N., 1989, ApJ 347, 1034
St.-Louis N., Drissen L., Moffat A.F.J., Bastien P., Tapia S., 1987, ApJ 322, 870
Taylor M., Nordsieck K.H., Schulte-Ladbeck R.E., Bjorkman K.S., 1991, AJ 102, 1187